Search for New Physics in All-hadronic Events with AlphaT in 8 TeV data at CERN

Yossof Eshaq

Submitted in Partial Fulfillment of the

Requirements for the Degree Doctor of Philosophy

Supervised by Professor Aran Garcia-Bellido

Department of Physics

Astronomy

Arts, Sciences and Engineering

University of Rocheser

September 21, 2014

Abstract

An inclusive search for supersymmetric processes that produce final states with jets and missing transverse energy is performed in pp collisions at a centre-of-mass energy of $\sqrt{s} = 8\,\text{TeV}$. The data sample corresponds to an integrated luminosity of 18.5 fb^{-1} collected by the CMS experiment at the LHC. In this search, a dimensionless kinematic variable, α_{T}, is used to discriminate between events with genuine and misreconstructed missing transverse energy. The search is based on an examination of the number of reconstructed jets per event, the scalar sum of transverse energies of these jets, and the number of these jets identified as originating from bottom quarks. The results are interpreted with various simplified models, with a special emphasis on models with a compressed mass spectrum.

0.1 Theoritical motivation

SM,Higgs,SUSY

Particle physics concerns itself with the study of particles and fields. Our current knowledge of their characterictics and interactions are formalized the quantum field theory called the Standard Model. I through three symmetries: The color charge symmetry of Quantum Chromo Dynamics (QCD) represented in SU(3), the flavor symemmetry of Quantum Flavor Dynamics (QFD) represented in SU(2) and the electric charge symmetry of Quantum Electro Dynamics represented in U(1). Together, SU(3)XSU(2)XU(1) represent the field theory.

0.2 LHC and CMS

LHC, CMS

0.3 Definition of $\alpha_{\mathbf{T}}$

0.4 Data sets and Monte Carlo samples

0.4.1 Data sets

0.4.2 MC samples for signal and SM backgrounds

0.4.3 Corrections to cross sections for SM samples

0.5 Triggers

0.5.1 Hadronic signal region

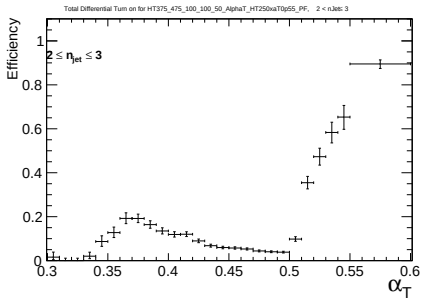

(a) Differential, $375 < H_{\mathrm{T}} < 475\,\mathrm{GeV}$

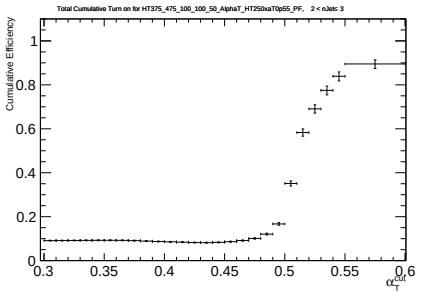

(b) Cumulative, $375 < H_{\mathrm{T}} < 475\,\mathrm{GeV}$

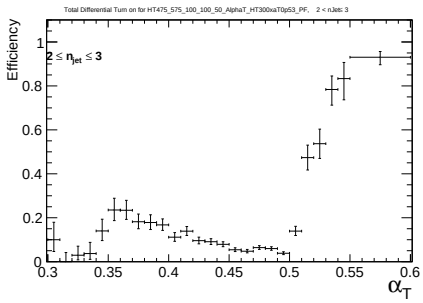

(c) Differential, $475 < H_{\mathrm{T}} < 525\,\mathrm{GeV}$

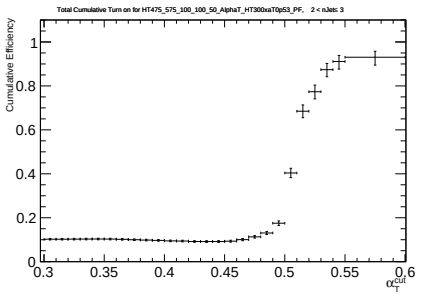

(d) Cumulative, $475 < H_{\mathrm{T}} < 525\,\mathrm{GeV}$

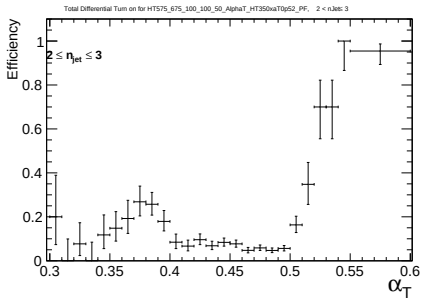

(e) Differential, $525 < H_{\mathrm{T}} < 675\,\mathrm{GeV}$

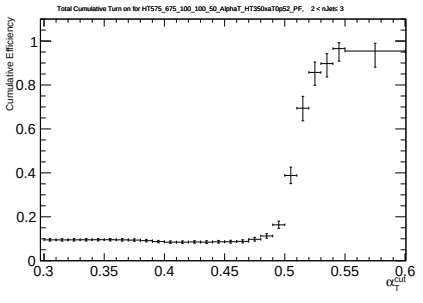

(f) Cumulative, $525 < H_{\mathrm{T}} < 675\,\mathrm{GeV}$

Figure 1: (Left) Differential and (Right) cumulative efficiency turn-on curves for the H_{T}-α_{T} cross triggers (as summarised in Table **??**) that record events for the three lowest H_{T} bins for events satisfying $2 \leq n_{\mathrm{jet}} \leq 3$.

0.5.2 Muon control samples

0.6 Physics objects

The definitions of the physics objects used in this analysis follow the recommendations of the various Physics Object Groups (POGs).

0.6.1 Jets

0.6.2 b-tagged jets

0.6.3 Muons

0.6.4 Photons

0.6.5 Electrons

0.6.6 Single isolated tracks

0.7 Event selection

0.7.1 Event vetoes for leptons, photons, and single isolated tracks

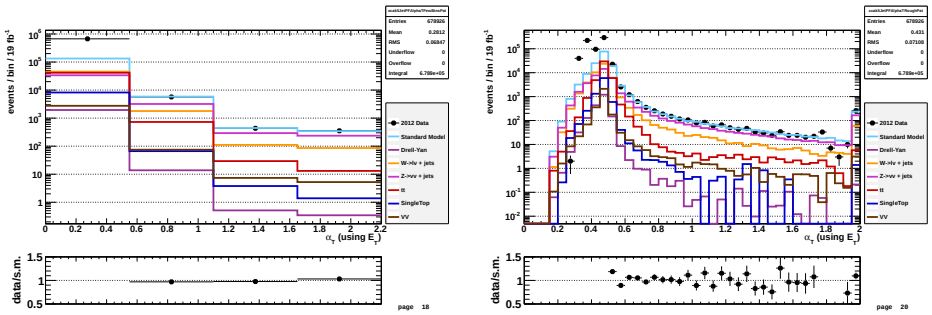

(a) (2–3,0) (b) (≥ 4,≥ 1)

Figure 2: Data–MC comparison of the α_{T} distribution for the hadronic signal region, following the application of the hadronic pre-selection criteria and the requirements $H_{\mathrm{T}} > 375\,\mathrm{GeV}$ and $\alpha_{\mathrm{T}} > 0.55$, for events satisfying (Left) $2 \leq n_{\mathrm{jet}} \leq 3$ and $n_{\mathrm{b}} = 0$ and (Right) $n_{\mathrm{jet}} \geq 4$ and $n_{\mathrm{b}} \geq 1$. Bands represent the uncertainties due to the limited size of MC samples.

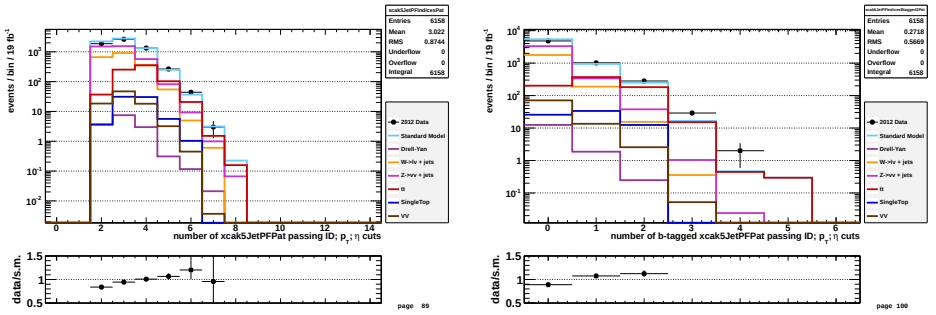

(a) n_{jet} distribution ($n_{\text{jet}} \geq 2$, $n_{\text{b}} \geq 0$).

(b) n_{b} distribution ($n_{\text{jet}} \geq 2$, $n_{\text{b}} \geq 0$)

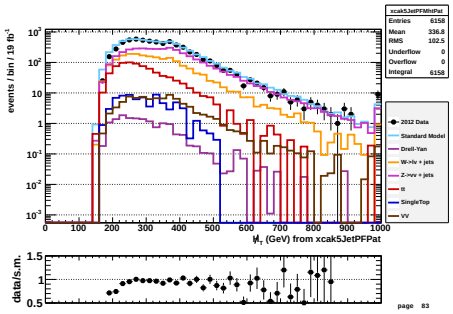

(c) H_{T} distribution ($n_{\text{jet}} \geq 2$, $n_{\text{b}} \geq 0$)

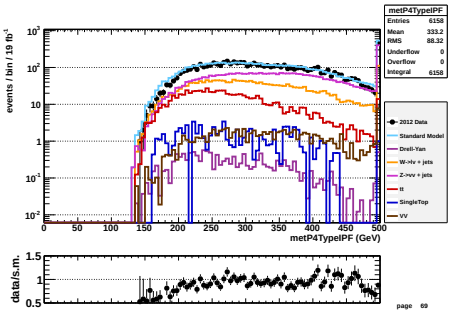

(d) H_{T} distribution ($n_{\text{jet}} \geq 2$, $n_{\text{b}} \geq 0$)

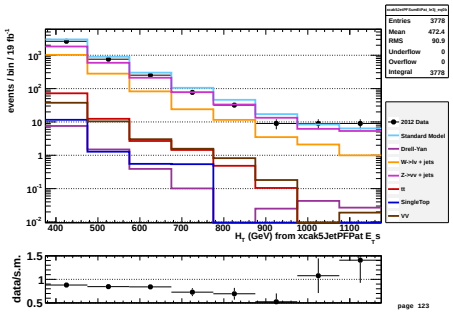

(e) H_{T} distribution ($2 \leq n_{\text{jet}} \leq 3$, $n_{\text{b}} = 0$)

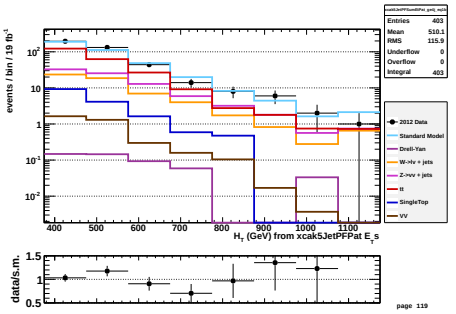

(f) H_{T} distribution ($n_{\text{jet}} \geq 4$, $n_{\text{b}} = 1$)

Figure 3: Data–MC comparisons of key variables for the hadronic signal region, following the application of the full signal region selection criteria and the requirements $H_{\text{T}} > 375\,\text{GeV}$ and $\alpha_{\text{T}} > 0.55$: (a) n_{jet}, (b) n_{b}, (c) H_{T}, and (d) $\not{E}_{\text{T}}$ distributions for an inclusive selection on n_{jet} and n_{b}, and (e,f) H_{T} for the two event categories ($2 \leq n_{\text{jet}} \leq 3$, $n_{\text{b}} = 0$) and ($n_{\text{jet}} \geq 4$, $n_{\text{b}} = 1$).

0.8 Closure tests and systematic uncertainties on transfer factors

Limitations in simulating detector effects and event kinematics requires us to apply appropriate systematics uncertainties on the simulation-based translation factors. The following section describes how we obatain these systematic uncertainty through the method of closure tests.

0.8.1 Closure tests

At its core, the method compares an observed yield (N_{obs}) and a predicted yield (N_{pred}) in a subsample of a control region. The predicted yield is constructed by translating from a statisically independent data sample to the data sample of interest by the use of the proper translation factor. For example, for a given HT bin, a prediction for the $n_{\text{jet}} \geq 4$, n_{b} =1, μ + jets sample can be made by translating from the $2 \leq n_{\text{jet}} \leq 3$, n_{b} =1, μ + jets in data via the translation factor:

$$\frac{N_{\text{MC}}^{\mu+\text{jets}}(H_{\text{T}}, n_{\text{jet}} \geq 4, n_{\text{b}} = 1)}{N_{\text{MC}}^{\mu+\text{jets}}(H_{\text{T}}, 2 \leq n_{\text{jet}} \leq 3, n_{\text{b}} = 1)} \tag{1}$$

The agreement betwen N_{obs} and N_{pred} is expressed as $(N_{\text{obs}} - N_{\text{pred}})/N_{\text{pred}}$. Assuming only statistical uncertainties on N_{obs} and N_{pred}, deviation of the ratio from zero defines our level of closure. A closure test set is defined as ratios for each bin. Looking at the ratio as a function of allows the measurment of statistical significant biases from zero and/or any dependence on . If statistically significant biases are observed, further studies are required to understand and correct for these biases.

Eight sets of closure tests probe key ingredients of the simulation modelling of the SM backgrounds with genuine $\boldsymbol{E}_{\text{T}}$ as a function of H_{T}, as shown in Fig. 4. This is done for the two jet multiplicity bins separately: (a) $2 \leq n_{\text{jet}} \leq 3$ and (b) $n_{\text{jet}} \geq 4$.

Under the assumption of closure for the full ensemble of tests, systematic uncertainties on the transfer factors are derived for each n_{jet} category and H_{T} regions. The treatment for estimating the

systematic uncertainties on the transfer factors is described in Section 0.8.2.

As described in section ?? The α_{T} requirement is not imposed in the μ + jets control sample. Therfore it is important to verify the approach of using μ + jets samples without an α_{T} requirement to make background predictions in the signal region. The first set of closure tests (denoted by cirlces) attempts to do this by probing the modelling of the α_{T} distribution in genuine $\not\!\!E_{\mathrm{T}}$ events as a function of H_{T}. The tests compares data yields in the μ + jets sample with an α_{T} requirement against predictions determined in a μ + jets sample with the α_{T} requirement inverted.

The next three sets (triangles, crosses, squares) probe the sensitivity of the transfer factors to the relative admixture of events from the W + jets and $t\bar{t}$ processes. These tests are conservative, since by construction, the admixture changes little when translating from the μ + jets control region to the signal region, whereas the closure tests use sub-samples with different b-tag requirements and therfore have very different admixtures of W + jets and $t\bar{t}$ events. In the $2 \leq n_{\mathrm{jet}} \leq 3$ bin, the test is sub-divided into seperate jet categories. These tests also probe the modelling of the reconstruction of b-quark jets, although this also addressed more fully by dedicated studies that determine systematic uncertainties via the method described in Sec. **??**.

The remaining tests probe the simulation modelling of the jet multiplicity in the μ + jets and γ + jets samples, which is checked due to the exclusive binning in jet multiplicity. As in the case of the W + jets / $t\bar{t}$ admixture, this set of tests is a very conservative check, as predictions are always made from the same jet multiplicity bin, whereas the closure tests translate between the two bins.

Tables 1 and 2, which summarize the results obtained from fits of zeroeth order polynomials (i.e. a constant) to the sets of closure tests performed in the $2 \leq n_{\mathrm{jet}} \leq 3$ and $n_{\mathrm{jet}} \geq 4$ bins. Table 3 lists the fits result common to both jet multiplicites. The best fit value and its uncertainty is listed for each set of closure tests, along with the χ^2, the number of degrees of freedom, and the p-value of the fit. The best fit value for the constant parameter is indicative of the level of closure, as averaged across the full H_{T} range considered in the analysis, and the p-value is indicative of

whether there is any significant dependence on H_{T}.

The closure tests demonstrate, within the statistical precision of each test, that there are no significant biases or dependencies on H_{T} inherent in the transfer factors obtained from simulation.

One set of tests does indicate a poor goodness of fit (indicated by a low p-value), which is the $n_{\mathrm{b}} = 0 \rightarrow n_{\mathrm{b}} = 1$ test in the μ + jets sample for the $n_{\mathrm{jet}} \geq 4$ category, which has been identified as a upward (downward) fluctuation of event counts in the H_{T} bin 475–575 GeV (575–675 GeV) when $n_{\mathrm{b}} = 1$. Combining these two bins yields an acceptable fit result, as indicated in Table 2, which points to a simple fluctuation rather than any systematic bias.

In addition to the fits described above, linear fits are also performed. The best fit values for the slope terms and the p-values obtained from each fit are summarised in Tables 1, 2, and 3. Typically, the best fit values are of the order 10^{-4}, which corresponds to a percent-level change per 100 GeV.

Table 1: A summary of the results obtained from fits of zeroeth order polynomials (i.e. a constant) to four sets of closure tests performed in the $2 \leq n_{\mathrm{jet}} \leq 3$ bin.

		Constant fit			
Closure test	Symbol	Best fit value	χ^2	d.o.f.	p-value
$\alpha_{\mathrm{T}} < 0.55 \rightarrow \alpha_{\mathrm{T}} > 0.55$ (μ + jets)	Circle	0.007 ± 0.02	3.91	7	0.79
1 b-tags $\rightarrow$2 b-tags (μ + jets, nJet=3)	Triangle	-0.008 ± 0.04	3.20	7	0.87
0 b-tags $\rightarrow$1 b-tags (μ + jets, nJet=2)	Cross	0.111 ± 0.03	5.87	7	0.55
0 b-tags $\rightarrow$1 b-tags (μ + jets, nJet=3)	Square	0.040 ± 0.02	1.12	7	0.99

Table 2: A summary of the results obtained from fits of zeroeth order polynomials (i.e. a constant) to three sets of closure tests performed in the $n_{\mathrm{jet}} \geq 4$ bin. †Further explanation of this fit can be found in the text.

		Constant fit			
Closure test	Symbol	Best fit value	χ^2	d.o.f.	p-value
$\alpha_{\mathrm{T}} < 0.55 \rightarrow \alpha_{\mathrm{T}} > 0.55$ (μ + jets)	Circle	0.011 ± 0.04	5.81	7	0.56
1 b-tags $\rightarrow$2 b-tags (μ + jets)	Triangle	0.045 ± 0.03	9.36	7	0.23
0 b-tags $\rightarrow$1 b-tags (μ + jets)	Square	0.007 ± 0.03	25.30	7	0.00
0 b-tags $\rightarrow$1 b-tags (μ + jets)†	Square	0.009 ± 0.03	10.12	6	0.12

Table 3: A summary of the results obtained from fits of zeroeth order polynomials (i.e. a constant) to four sets of closure tests ($2 \leq n_{\text{jet}} \leq 3 \rightarrow n_{\text{jet}} \geq 4$) that probe the accuracy of the MC modelling of the n_{jet} distribution observed in data, using the three data control samples.

		Constant fit			
Closure test	Symbol	Best fit value	χ^2	d.o.f.	p-value
$2 \leq n_{\text{jet}} \leq 3 \rightarrow n_{\text{jet}} \geq 4$ (μ + jets, 1 b-tags)	Times	-0.053 ± 0.03	8.02	7	0.33
$2 \leq n_{\text{jet}} \leq 3 \rightarrow n_{\text{jet}} \geq 4$ (μ + jets, 1 b-tags)	Invert. Triangle	0.018 ± 0.04	6.23	7	0.51
$2 \leq n_{\text{jet}} \leq 3 \rightarrow n_{\text{jet}} \geq 4$ (μ + jets, 0 b-tags)	Star	0.034 ± 0.02	9.24	7	0.24
$2 \leq n_{\text{jet}} \leq 3 \rightarrow n_{\text{jet}} \geq 4$ (γ + jets, 0 b-tags)	Diamond	0.100 ± 0.04	12.20	7	0.09

0.8.2 Systematic uncertainties from closure tests

Once it is established that no significantly large bias or trend is observed for any set of closure tests, then systematic uncertainties are determined.

Systematics are determined for each H_{T} bin,as indicated in Table 4. For each H_{T} region, the systematic uncertainty is estimated by taking the quadrature sum of the weighted mean and sample variance for the closure tests within the given H_{T} region. This procedure yields the values quoted in Table 4.

The effect of uncertainties related to the modelling of b-quark jets in simulation on the transfer factors is found to be negligible, at the percent level as discussed in Section **??**, in comparison to the aforementioned n_{jet}- and H_{T}-dependent systematic uncertainties.

Table 4: A summary of the magnitude of the systematic uncertainties (%) assigned to the transfer factors, according to n_{jet} and H_{T} region.

	H_{T} region (GeV)							
n_{jet}	375–475	475–525	525–675	675–775	775–875	875-975	1075-1075	> 1175
2–3	3	4	5	11	11	16	16	16
$\geq$4	3	4	6	13	13	13	13	20

Figure 4 shows the sets of closure tests overlaid on top of grey bands that represent the H_{T}-dependent systematic uncertainties in Table 4. These systematic uncertainties are assumed to fully

uncorrelated between the different b jet multiplicity categories and also the seven H_{T} regions, which is a conservative approach given that one can expect some correlation between adjacent H_{T} bins (due to comparable kinematics). This approach of decorrelating the H_{T} regions should be contrasted against the fits shown in Figure **??** that do assume a correlated behaviour in H_{T}.

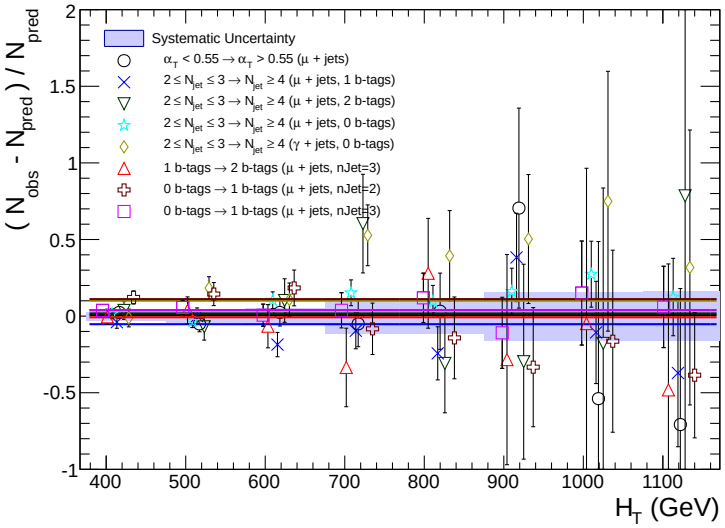

(a) $2 \le n_{\text{jet}} \le 3$

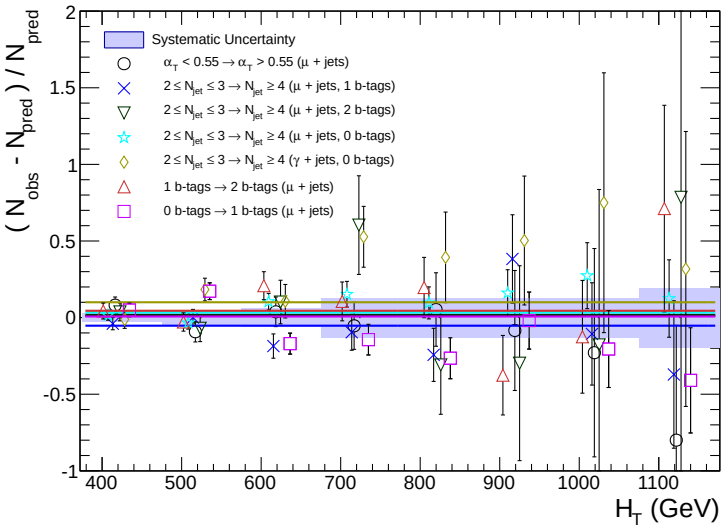

(b) $n_{\text{jet}} \ge 4$

Figure 4: Sets of closure tests (open symbols) overlaid on top of the systematic uncertainty used for each of the five H_{T} regions (shaded bands) and for the two different jet multiplicity bins: (a) $2 \le n_{\text{jet}} \le 3$ and (b) $n_{\text{jet}} \ge 4$.

0.9 Results

0.9.1 Standard Model

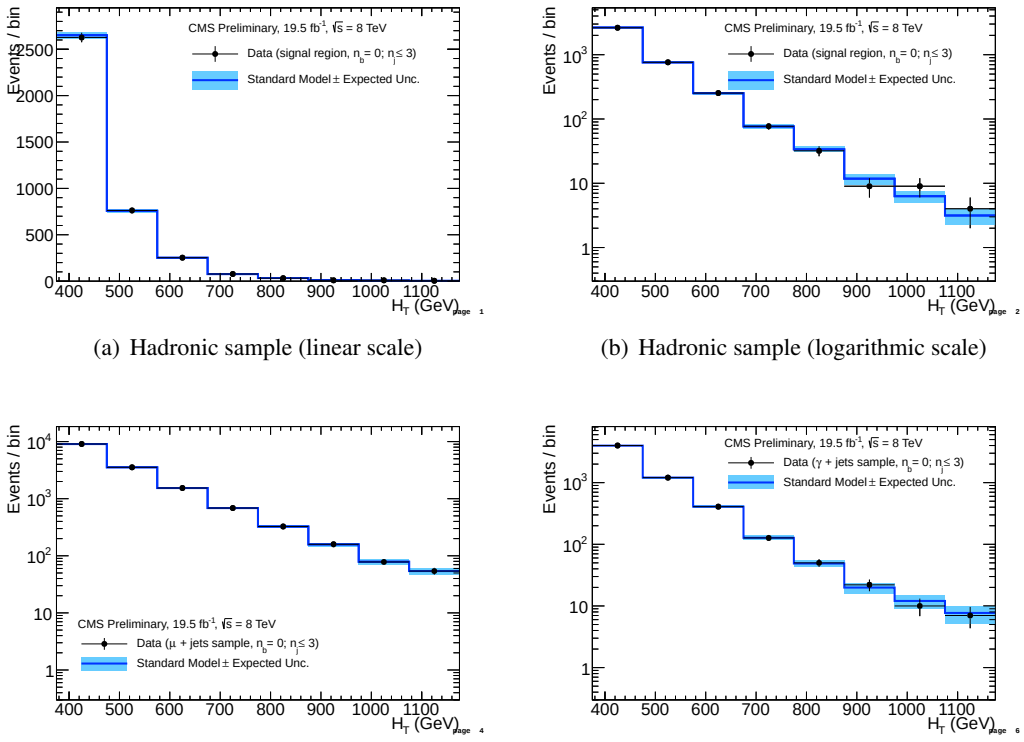

(a) Hadronic sample (linear scale)

(b) Hadronic sample (logarithmic scale)

(c) μ + jets sample

(d) γ + jets sample

Figure 5: Comparison of the H_{T}-binned observed data yields and SM expectations when requiring $2 \leq n_{\mathrm{jet}} \leq 3$ and $n_{\mathrm{b}} = 0$ for the (a-b) hadronic, (c) μ + jets, (d) $\mu\mu$ + jets and (e) γ + jets samples, as determined by a simultaneous fit to all data samples under the SM-only hypothesis. The observed event yields in data (black dots) and the expectations and their uncertainties (dark blue solid line with light blue bands), as determined by the simultaneous fit, are shown. For illustrative purposes only, the signal expectations (pink dashed line) for the model T2cc with $m_{\tilde{\mathrm{q}}} = 250\,\mathrm{GeV}$ and $m_{\mathrm{LSP}} = 240\,\mathrm{GeV}$ are stacked on top of the SM expectations.

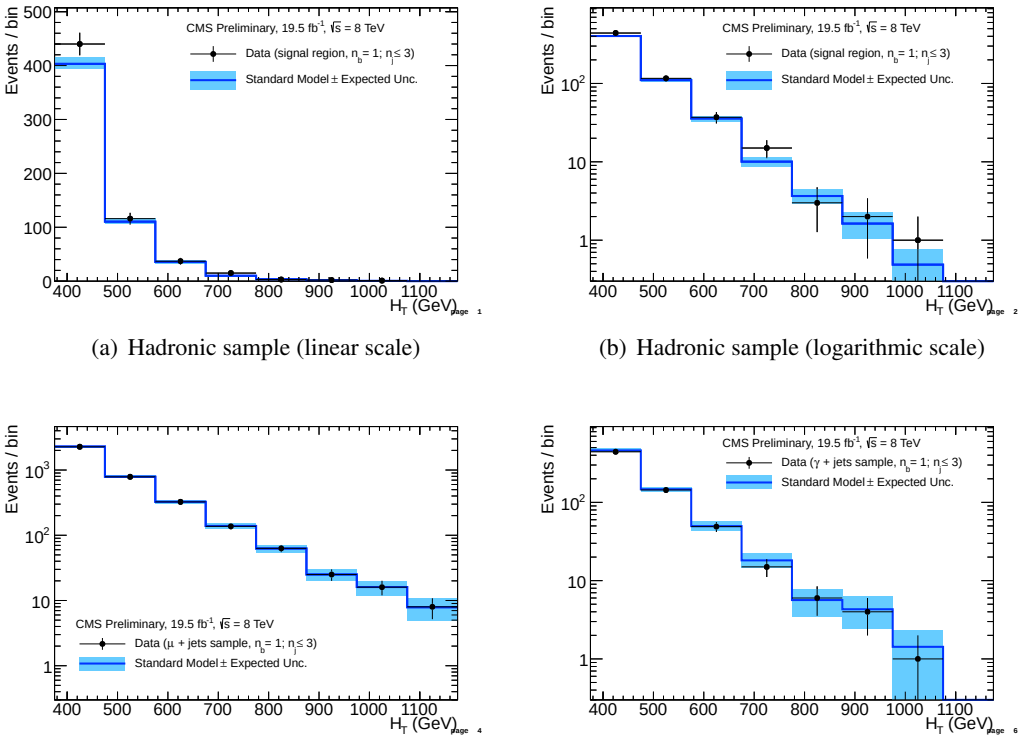

(a) Hadronic sample (linear scale)

(b) Hadronic sample (logarithmic scale)

(c) μ + jets sample

(d) γ + jets sample

Figure 6: Comparison of the H_{T}-binned observed data yields and SM expectations when requiring $2 \leq n_{\mathrm{jet}} \leq 3$ and $n_{\mathrm{b}} = 1$ for the (a-b) hadronic, (c) μ + jets, (d) $\mu\mu$ + jets and (e) γ + jets samples, as determined by a simultaneous fit to all data samples under the SM-only hypothesis. The observed event yields in data (black dots) and the expectations and their uncertainties (dark blue solid line with light blue bands), as determined by the simultaneous fit, are shown. For illustrative purposes only, the signal expectations (pink dashed line) for the model T2cc with $m_{\tilde{\mathrm{q}}} = 250\,\mathrm{GeV}$ and $m_{\mathrm{LSP}} = 170\,\mathrm{GeV}$ are stacked on top of the SM expectations.

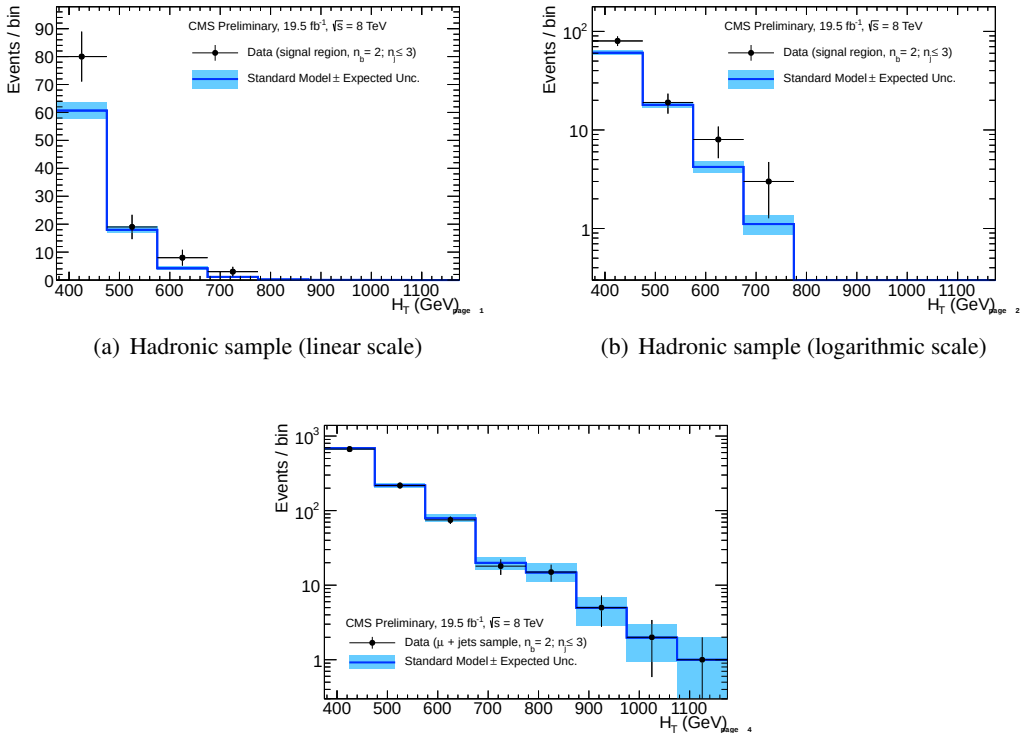

(a) Hadronic sample (linear scale)

(b) Hadronic sample (logarithmic scale)

(c) μ + jets sample

Figure 7: Comparison of the H_{T}-binned observed data yields and SM expectations when requiring $2 \leq n_{\mathrm{jet}} \leq 3$ and $n_{\mathrm{b}} = 2$ for the (a-b) hadronic and μ + jets samples, as determined by a simultaneous fit to both the hadronic and μ + jets data samples under the SM-only hypothesis. The observed event yields in data (black dots) and the expectations and their uncertainties (dark blue solid line with light blue bands), as determined by the simultaneous fit, are shown.

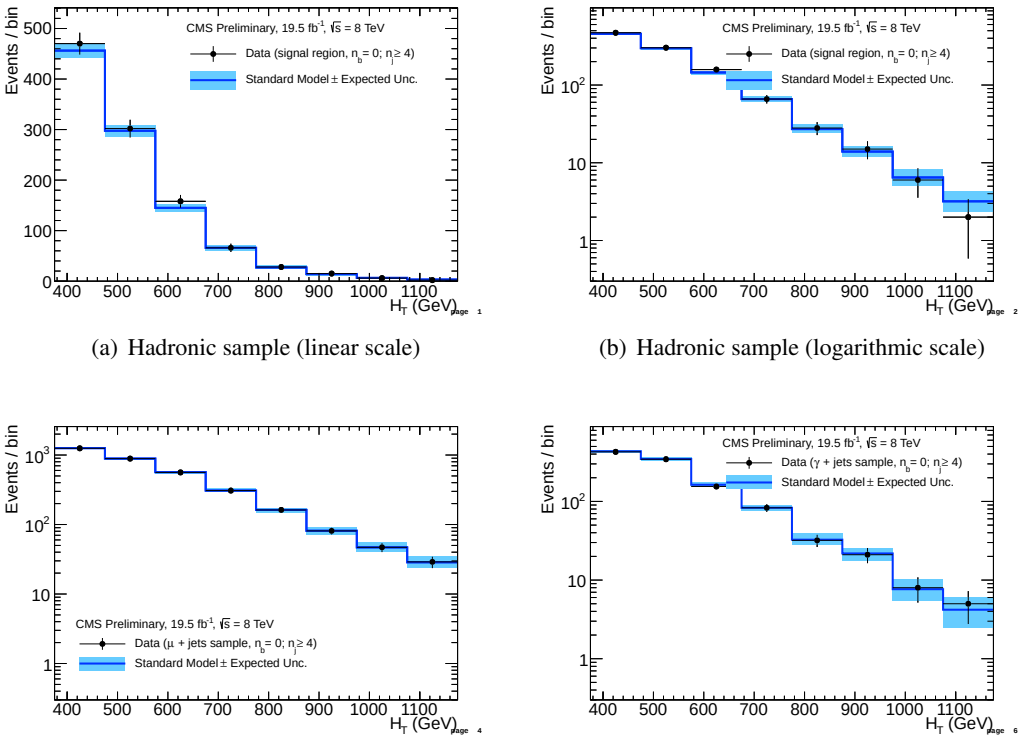

(a) Hadronic sample (linear scale)

(b) Hadronic sample (logarithmic scale)

(c) μ + jets sample

(d) γ + jets sample

Figure 8: Comparison of the H_{T}-binned observed data yields and SM expectations when requiring $n_{\mathrm{jet}} \geq 4$ and $n_{\mathrm{b}} = 0$ for the (a-b) hadronic, (c) μ + jets, (d) $\mu\mu$ + jets and (e) γ + jets samples, as determined by a simultaneous fit to all data samples under the SM-only hypothesis. The observed event yields in data (black dots) and the expectations and their uncertainties (dark blue solid line with light blue bands), as determined by the simultaneous fit, are shown. For illustrative purposes only, the signal expectations (pink dashed line) for the model T2cc with $m_{\tilde{\mathrm{q}}} = 250\,\mathrm{GeV}$ and $m_{\mathrm{LSP}} = 170\,\mathrm{GeV}$ are stacked on top of the SM expectations.

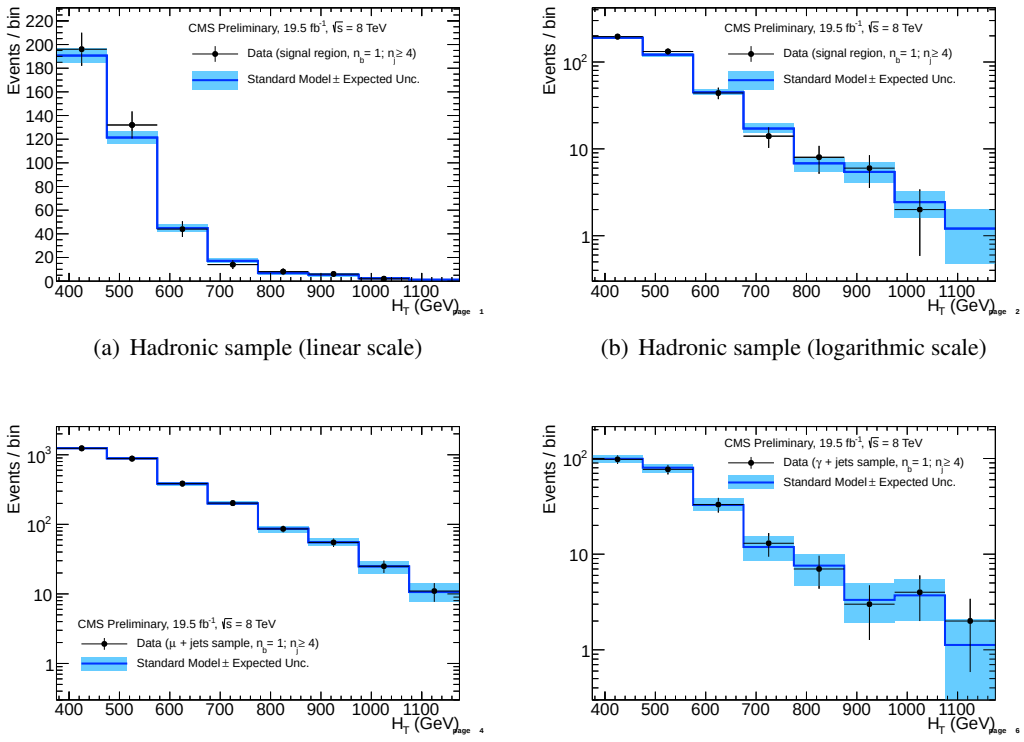

(a) Hadronic sample (linear scale)

(b) Hadronic sample (logarithmic scale)

(c) μ + jets sample

(d) γ + jets sample

Figure 9: Comparison of the H_{T}-binned observed data yields and SM expectations when requiring $n_{\mathrm{jet}} \geq 4$ and $n_{\mathrm{b}} = 1$ for the (a-b) hadronic, (c) μ + jets, (d) $\mu\mu$ + jets and (e) γ + jets samples, as determined by a simultaneous fit to all data samples under the SM-only hypothesis. The observed event yields in data (black dots) and the expectations and their uncertainties (dark blue solid line with light blue bands), as determined by the simultaneous fit, are shown. For illustrative purposes only, the signal expectations (pink dashed line) for the model T2cc with $m_{\tilde{\mathrm{q}}} = 250\,\mathrm{GeV}$ and $m_{\mathrm{LSP}} = 170\,\mathrm{GeV}$ are stacked on top of the SM expectations.

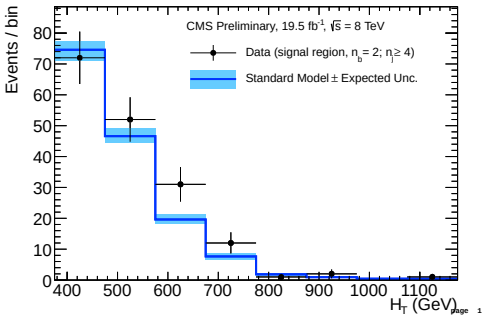

(a) Hadronic sample (linear scale)

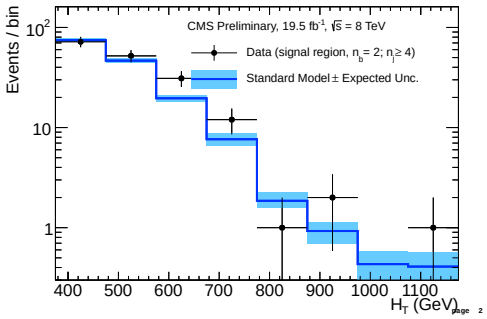

(b) Hadronic sample (logarithmic scale)

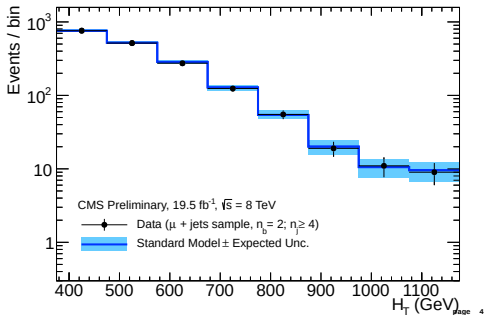

(c) μ + jets sample

Figure 10: Comparison of the H_T-binned observed data yields and SM expectations when requiring $n_{jet} \geq 4$ and $n_b = 2$ for the (a-b) hadronic and μ + jets samples, as determined by a simultaneous fit to both the hadronic and μ + jets data samples under the SM-only hypothesis. The observed event yields in data (black dots) and the expectations and their uncertainties (dark blue solid line with light blue bands), as determined by the simultaneous fit, are shown.

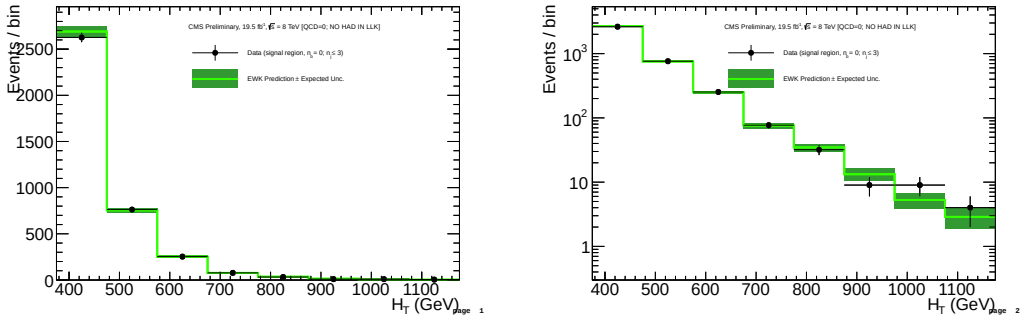

(a) Hadronic sample (linear scale)

(b) Hadronic sample (logarithmic scale)

(c) μ + jets sample

(d) γ + jets sample

Figure 11: Comparison of the H_{T}-binned observed data yields and SM expectations when requiring $2 \leq n_{\mathrm{jet}} \leq 3$ and $n_{\mathrm{b}} = 0$ for the (a-b) hadronic, (c) μ + jets, (d) $\mu\mu$ + jets and (e) γ + jets samples, as determined by a simultaneous fit to the data control samples only. The observed event yields in data (black dots) and the expectations and their uncertainties (dark green solid line with light green bands), as determined by the simultaneous fit, are shown.

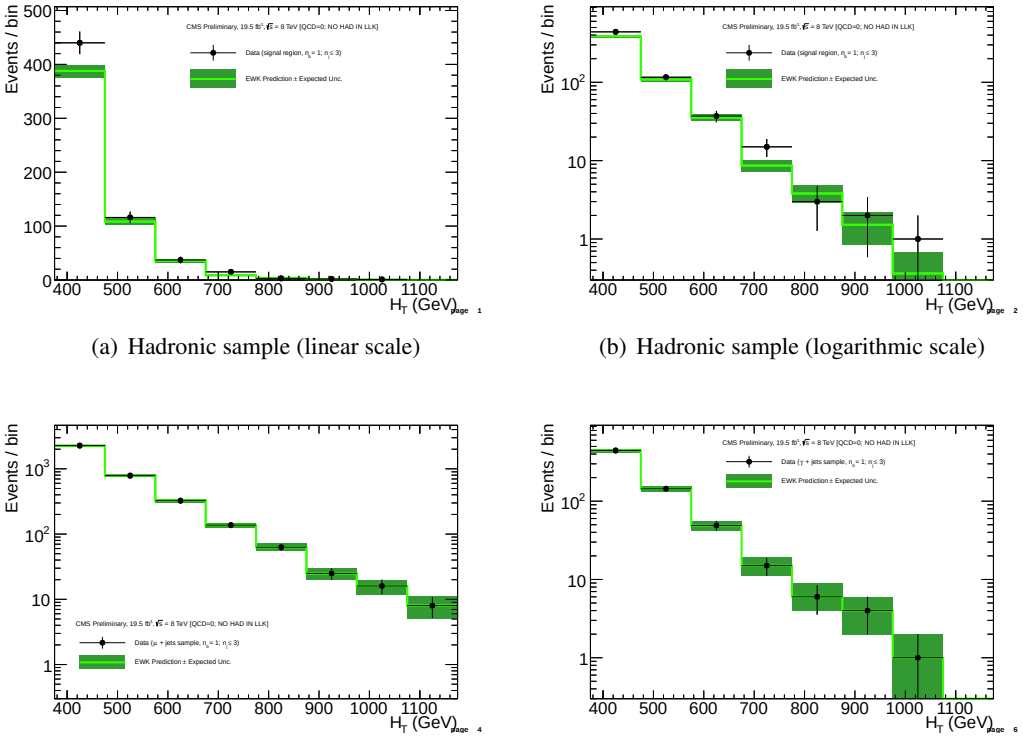

(a) Hadronic sample (linear scale)

(b) Hadronic sample (logarithmic scale)

(c) μ + jets sample

(d) γ + jets sample

Figure 12: Comparison of the H_{T}-binned observed data yields and SM expectations when requiring $2 \leq n_{\mathrm{jet}} \leq 3$ and $n_{\mathrm{b}} = 1$ for the (a-b) hadronic, (c) μ + jets, (d) $\mu\mu$ + jets and (e) γ + jets samples, as determined by a simultaneous fit to the data control samples only. The observed event yields in data (black dots) and the expectations and their uncertainties (dark green solid line with light green bands), as determined by the simultaneous fit, are shown.

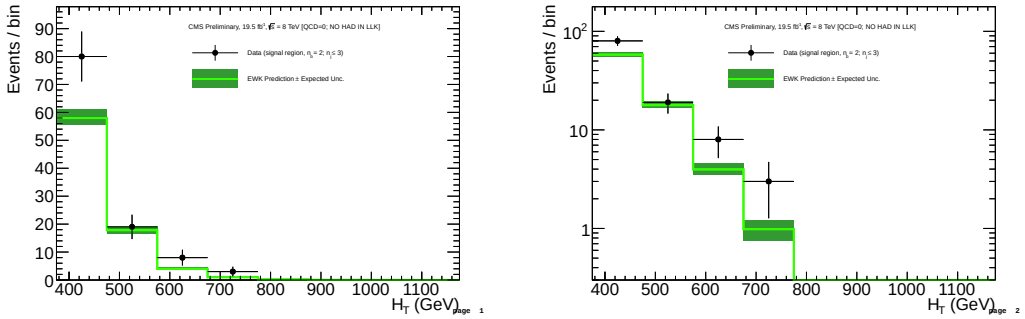

(a) Hadronic sample (linear scale)

(b) Hadronic sample (logarithmic scale)

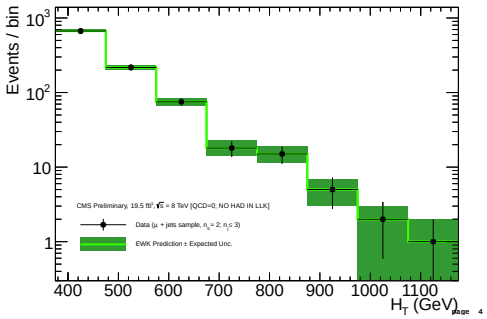

(c) μ + jets sample

Figure 13: Comparison of the H_{T}-binned observed data yields and SM expectations when requiring $2 \leq n_{\mathrm{jet}} \leq 3$ and $n_{\mathrm{b}} = 2$ for the (a-b) hadronic, (c) μ + jets, (d) $\mu\mu$ + jets and (e) γ + jets samples, as determined by the μ + jets data control sample only. The observed event yields in data (black dots) and the expectations and their uncertainties (dark green solid line with light green bands) are shown.

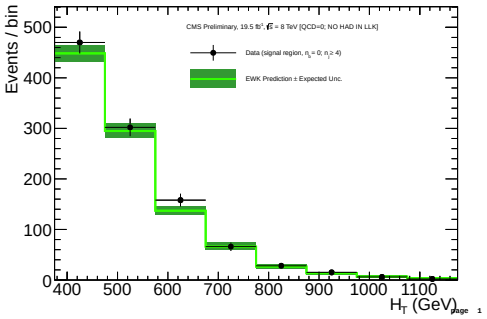

(a) Hadronic sample (linear scale)

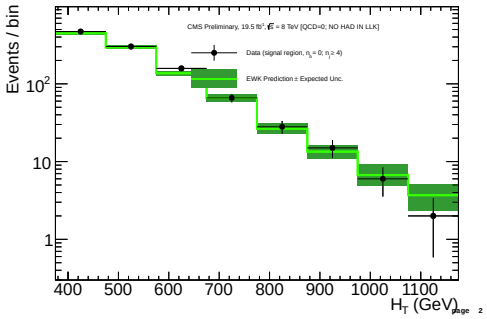

(b) Hadronic sample (logarithmic scale)

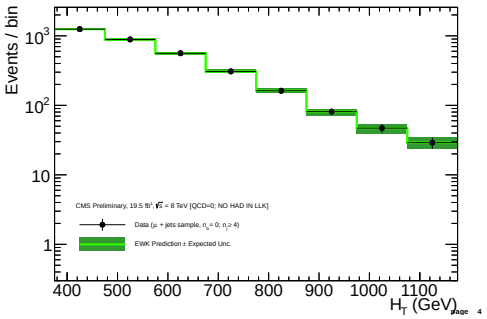

(c) μ + jets sample

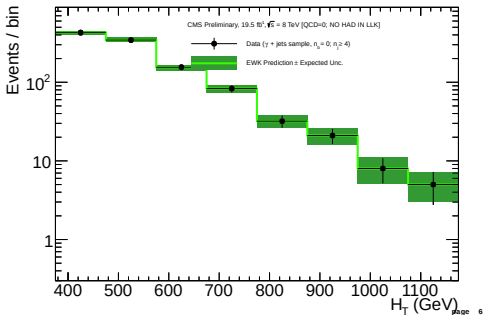

(d) γ + jets sample

Figure 14: Comparison of the H_{T}-binned observed data yields and SM expectations when requiring $n_{\mathrm{jet}} \geq 4$ and $n_{\mathrm{b}} = 0$ for the (a-b) hadronic, (c) μ + jets, (d) $\mu\mu$ + jets and (e) γ + jets samples, as determined by a simultaneous fit to the data control samples only. The observed event yields in data (black dots) and the expectations and their uncertainties (dark green solid line with light green bands), as determined by the simultaneous fit, are shown.

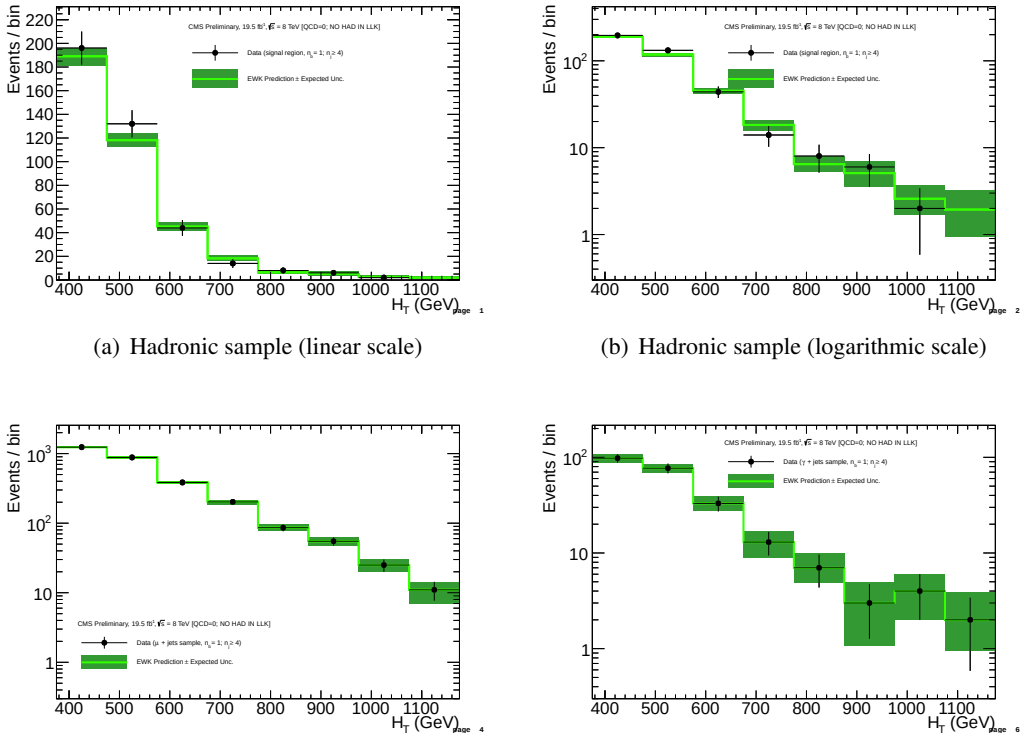

(a) Hadronic sample (linear scale)

(b) Hadronic sample (logarithmic scale)

(c) μ + jets sample

(d) γ + jets sample

Figure 15: Comparison of the H_{T}-binned observed data yields and SM expectations when requiring $n_{\mathrm{jet}} \geq 4$ and $n_{\mathrm{b}} = 1$ for the (a-b) hadronic, (c) μ + jets, (d) $\mu\mu$ + jets and (e) γ + jets samples, as determined by a simultaneous fit to the data control samples only. The observed event yields in data (black dots) and the expectations and their uncertainties (dark green solid line with light green bands), as determined by the simultaneous fit, are shown.

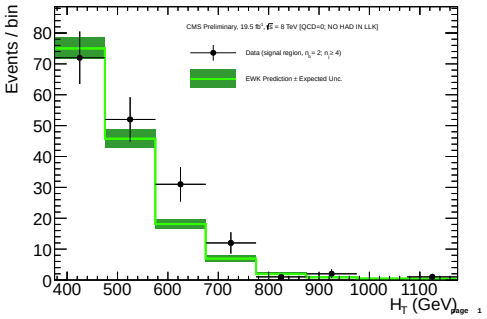

(a) Hadronic sample (linear scale)

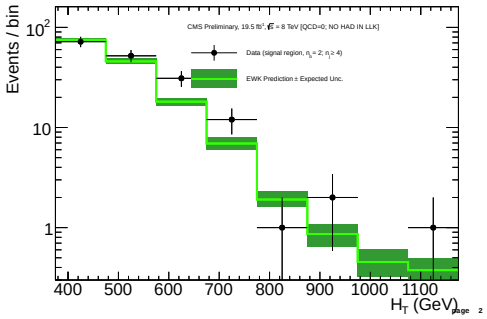

(b) Hadronic sample (logarithmic scale)

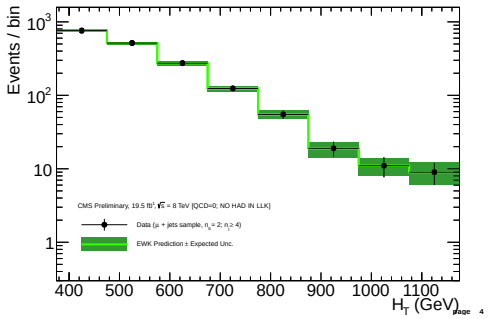

(c) μ + jets sample

Figure 16: Comparison of the H_{T}-binned observed data yields and SM expectations when requiring $n_{\mathrm{jet}} \geq 4$ and $n_{\mathrm{b}} = 2$ for the (a-b) hadronic, (c) μ + jets, (d) $\mu\mu$ + jets and (e) γ + jets samples, as determined by the μ + jets data control sample only. The observed event yields in data (black dots) and the expectations and their uncertainties (dark green solid line with light green bands) are shown.

.1 SM-only yield tables

The following tables compare the observations in the hadronic and control samples with the maximum-likelihood expectations obtained by the SM-only fit.

Table 5: 0b le3j

H_{T} Bin (GeV)	375–475	475–575	575–675	675–775	775–875	875–975	975–1075	1075–∞
SM hadronic	2652^{+33}_{-41}	758^{+20}_{-18}	252^{+10}_{-12}	$76.5^{+6.1}_{-5.0}$	$33.7^{+3.2}_{-3.3}$	$11.8^{+2.0}_{-2.2}$	$6.3^{+1.4}_{-1.3}$	$3.2^{+0.9}_{-0.9}$
Data hadronic	2627	762	253	77	32	9	9	4
SM μ+jets	9069^{+77}_{-115}	3546^{+51}_{-59}	1538^{+33}_{-39}	686^{+22}_{-27}	325^{+18}_{-16}	158^{+12}_{-13}	$78.6^{+6.2}_{-9.4}$	$54.1^{+7.5}_{-7.3}$
Data μ+jets	9078	3545	1538	686	326	159	78	54
SM γ+jets	3984^{+56}_{-59}	1209^{+34}_{-35}	408^{+17}_{-22}	127^{+10}_{-9}	$48.8^{+6.0}_{-5.5}$	$19.9^{+3.8}_{-3.9}$	$12.1^{+2.8}_{-3.1}$	$7.7^{+2.4}_{-2.5}$
Data γ+jets	4000	1206	408	127	50	22	10	7

Table 6: 0b ge4j

H_{T} Bin (GeV)	375–475	475–575	575–675	675–775	775–875	875–975	975–1075	1075–∞
SM hadronic	456^{+13}_{-14}	298^{+12}_{-12}	145^{+7}_{-7}	$66.0^{+5.5}_{-4.7}$	$27.1^{+3.8}_{-3.1}$	$13.9^{+2.2}_{-2.1}$	$6.5^{+1.8}_{-1.4}$	$3.2^{+1.0}_{-0.9}$
Data hadronic	470	302	158	66	28	15	6	2
SM μ+jets	1256^{+30}_{-41}	890^{+28}_{-30}	567^{+22}_{-23}	308^{+18}_{-15}	162^{+12}_{-12}	$81.3^{+9.9}_{-9.3}$	$46.9^{+7.8}_{-6.5}$	$28.6^{+6.7}_{-4.8}$
Data μ+jets	1249	888	562	308	162	81	47	29
SM γ+jets	434^{+19}_{-18}	347^{+15}_{-18}	163^{+12}_{-11}	$83.0^{+6.8}_{-7.5}$	$32.6^{+6.3}_{-5.0}$	$21.8^{+4.1}_{-4.1}$	$7.7^{+2.5}_{-2.3}$	$4.2^{+1.8}_{-1.8}$
Data γ+jets	427	344	155	83	32	21	8	5

Table 7: 1b le3j

H_{T} Bin (GeV)	375–475	475–575	575–675	675–775	775–875	875–975	975–1075	1075–∞
SM hadronic	403^{+12}_{-10}	110^{+6}_{-5}	$35.8^{+2.9}_{-2.9}$	$10.0^{+1.5}_{-1.3}$	$3.7^{+0.8}_{-0.8}$	$1.6^{+0.6}_{-0.6}$	$0.5^{+0.3}_{-0.3}$	$0.1^{+0.1}_{-0.0}$
Data hadronic	440	116	37	15	3	2	1	0
SM μ+jets	2291^{+50}_{-48}	790^{+31}_{-25}	326^{+20}_{-16}	139^{+13}_{-11}	$62.7^{+8.3}_{-7.4}$	$25.1^{+4.7}_{-5.0}$	$16.1^{+3.9}_{-4.2}$	$7.9^{+3.0}_{-3.0}$
Data μ+jets	2272	787	325	137	63	25	16	8
SM γ+jets	461^{+22}_{-22}	147^{+10}_{-10}	$49.7^{+6.5}_{-6.7}$	$18.1^{+4.0}_{-3.6}$	$5.6^{+2.0}_{-2.2}$	$4.3^{+2.0}_{-1.9}$	$1.4^{+0.9}_{-1.4}$	$0.0^{+0.0}_{--0.0}$
Data γ+jets	444	144	49	15	6	4	1	0

Table 8: 1b ge4j

H_{T} Bin (GeV)	375–475	475–575	575–675	675–775	775–875	875–975	975–1075	1075–∞
SM hadronic	191^{+6}_{-6}	121^{+5}_{-5}	$44.8^{+3.3}_{-2.8}$	$17.1^{+2.3}_{-1.9}$	$6.8^{+1.1}_{-1.3}$	$5.4^{+1.5}_{-1.4}$	$2.4^{+0.8}_{-0.8}$	$1.2^{+0.8}_{-0.7}$
Data hadronic	196	132	44	14	8	6	2	0
SM μ+jets	1242^{+37}_{-34}	888^{+27}_{-26}	384^{+21}_{-18}	200^{+14}_{-12}	$86.6^{+9.1}_{-10.0}$	$55.2^{+7.4}_{-6.2}$	$24.9^{+4.6}_{-5.7}$	$10.6^{+3.3}_{-3.0}$
Data μ+jets	1238	881	385	202	86	55	25	11
SM γ+jets	$99.2^{+9.5}_{-8.6}$	$80.2^{+7.9}_{-8.7}$	$32.7^{+5.7}_{-4.6}$	$11.9^{+3.4}_{-3.3}$	$7.6^{+2.3}_{-2.9}$	$3.3^{+1.7}_{-1.4}$	$3.7^{+1.8}_{-1.7}$	$1.1^{+1.0}_{-1.0}$
Data γ+jets	98	77	33	13	7	3	4	2

Table 9: 2b le3j

H_{T} Bin (GeV)	375–475	475–575	575–675	675–775	775–875	875–975	975–1075	1075–∞
SM hadronic	$60.7^{+2.9}_{-3.1}$	$18.0^{+1.3}_{-1.2}$	$4.2^{+0.6}_{-0.5}$	$1.1^{+0.2}_{-0.2}$	$0.2^{+0.1}_{-0.1}$	$0.0^{+0.0}_{-0.0}$	$0.0^{+0.0}_{-0.0}$	$0.0^{+0.0}_{-0.0}$
Data hadronic	80	19	8	3	0	0	0	0
SM μ+jets	687^{+23}_{-26}	218^{+14}_{-14}	$78.8^{+9.1}_{-8.5}$	$19.9^{+3.9}_{-3.9}$	$14.8^{+4.9}_{-3.8}$	$5.0^{+2.0}_{-2.1}$	$2.0^{+1.0}_{-1.0}$	$1.0^{+1.0}_{-1.0}$
Data μ+jets	668	217	75	18	15	5	2	1

Table 10: 2b ge4j

H_{T} Bin (GeV)	375–475	475–575	575–675	675–775	775–875	875–975	975–1075	1075–∞
SM hadronic	$74.6^{+3.0}_{-3.5}$	$46.6^{+2.5}_{-2.3}$	$19.6^{+1.6}_{-1.4}$	$7.6^{+1.2}_{-1.1}$	$1.9^{+0.4}_{-0.3}$	$0.9^{+0.2}_{-0.2}$	$0.4^{+0.1}_{-0.1}$	$0.4^{+0.2}_{-0.1}$
Data hadronic	72	52	31	12	1	2	0	1
SM μ+jets	757^{+23}_{-28}	520^{+23}_{-21}	285^{+18}_{-15}	128^{+10}_{-10}	$54.1^{+8.8}_{-5.8}$	$20.1^{+4.1}_{-4.7}$	$10.6^{+3.0}_{-3.0}$	$9.6^{+2.9}_{-2.9}$
Data μ+jets	760	515	274	124	55	19	11	9

Bibliography

[1] S. Chatrchyan et al. Missing transverse energy performance of the cms detector. *JINST*, 6:P09001, 2011.

[2] Serguei Chatrchyan et al. Determination of Jet Energy Calibration and Transverse Momentum Resolution in CMS. *JINST*, 6:P11002, 2011.

[3] V. Khachatryan et al. Search for Supersymmetry in pp Collisions at 7 TeV in Events with Jets and Missing Transverse Energy. *Phys. Lett. B*, 698:196, 2011.

[4] L. Randall and D. Tucker-Smith. Dijet searches for supersymmetry at the large hadron collider. *Phys. Rev. Lett.*, 101:221803, 2008.